Silk fibroin hydrogels for potential applications in photodynamic therapy

Jose Eduardo U. Rojas,[a] Barbara B. Gerbelli,[a] Anderson O. Ribeiro,[a] Iseli L. Nantes-Cardoso,[a] Francesca Giuntini,[b] Wendel A. Alves[a]*

[a]*Centro de Ciências Naturais e Humanas, Universidade Federal do ABC, 09210-580, Santo André, Brazil;*

[b]*School of Pharmacy and Biomolecular Sciences, Liverpool John Moores University, Byrom Street, Liverpool, L3 3AF, UK.*

Abstract

In this study, we prepared translucid hydrogels with different concentrations of silk fibroin, extracted from raw silk fibers, and used them as a matrix to incorporate the photosensitizer 5-(4-aminophenyl)-10,15,20-tris-(4-sulphonatophenyl) porphyrin trisodium for application in photodynamic therapy (PDT). The hydrogels obtained were characterized by rheology, spectrophotometry and scattering techniques to elucidate the factors involved in the formation of the hydrogel, and to characterize the behavior of silk fibroin (SF) after incorporating of the porphyrin to the matrix. The rheology results demonstrated that the SF hydrogels had a shear thinning behavior. In addition, we were able to verify that the structure of the material was able to be recovered over time after shear deformation. The encapsulation of porphyrins in hydrogels leads to the formation of self-assembled peptide nanostructures that prevent porphyrin aggregation, thereby greatly increasing the generation of singlet oxygen. Also, our findings suggest that porphyrin can diffuse out of the hydrogel and permeate the outer skin layers. This evidence suggests that SF hydrogels could be used as porphyrin encapsulation and as a drug carrier for the sustained release of photosensitizers for PDT.

Keywords: *porphyrin, fibroin, hydrogel, photodynamic therapy, rheology, singlet oxygen.*

Introduction

Currently, studies on natural polymers have increased notably due to their biocompatibility and exceptional physical and chemical properties, which would be difficult to obtain by a synthetic route.[1] Among these natural polymers, silk fibroin (SF) is attractive because of its optical transparency, outstanding mechanical robustness and biocompatibility, and also because they can form non-inflammatory degradation products.[2] The characteristic of silk structure with uniform protein content and thread makes this material an ideal option for the non-absorbable sutures in a wide range of wound closures.[3] The remarkable properties of fibroin allow this material to be processed into many different forms, including films, sponges, hydrogels, microparticles, microspheres , microneedles and others.[4-6]

Hydrogels prepared from SF have the potential to overcome some of the limitations of hydrogels that are prepared from synthetic polymers, namely, unfavorable mechanical and thermal properties, the presence of unreacted monomers and the use of toxic cross linkers.[7] In addition to being used for cell culture and in the formation of different biomedical devices, hydrogels can act as biocompatible and biodegradable matrices for the transport and selective release of drugs or other biologically active compounds,[8] which significantly expands the physical potential and applications, such as SF-based drug delivery systems.[9] SF has been used for the controlled delivery of a variety of therapeutic agents, but to the best of our knowledge, the SF-mediated delivery of photosensitizers has not been explored to date.

Photodynamic therapy is a clinically approved, minimally invasive therapeutic procedure that exerts selective cytotoxic activity toward malignant cells. The procedure involves the administration of a photosensitizing agent (photosensitizer) followed by irradiation at a wavelength corresponding to an absorbance band of the photosensitizer, leading to the generation of reactive oxygen species (ROS) to promote the death of malignant cell, infectious agents, and removal of burns.[10–12] PDT has numerous advantages over typical cancer treatment, such as surgery, chemotherapy and radiotherapy. Additionally, PDT is relatively non-invasive, as it requires irradiation of the tumor site with visible light, thereby inducing minimal injury to the adjacent normal tissues. PDT does not induce systemic immunosuppressive effects that may lead to clinical opportunistic infections, and it can be repeatedly administered without detrimental consequences to the patient.[13,14]

Despite the many positive features of PDT in cancer therapy, its translation to a clinical setting remains slow; this can in part be due to the peculiar physicochemical properties of photosensitizing agents.[15] Most known photosensitizers are hydrophobic and sparingly soluble in water, which explains why numerous nanoplatforms based on organic (*e.g.*, proteins, smarts self-assembly peptides, nanodots, submicron and nanoparticles).[16-19] and inorganic materials have been investigated for targeted and non-targeted photosensitizer delivery.[20] For targeted PDT, functionalized nanomaterials are required to efficiently incorporate and deliver hydrophobic PS drugs only to target tissues/cells and to activate them for ROS production.[21] In addition, functionalized nanomaterials must be biocompatible, transparent or translucid, to allow the penetration of light, and have sufficient photosensitizer-loading capacity. The lack of transparency of SF hydrogels has been a hindrance to fully exploit this material format for the incorporation of light-sensitive molecules (*e.g.*, fluorescent, bioluminescent or photoactive macromolecules) into hydrogels to sensing and diagnostic applications and PDT.[22]

Herein, we report on the extraction of pure fibroin from raw silk fibers and the synthetize and characterization of transparent fibroin hydrogels, as well the use of such hydrogels as matrices to incorporate the water-soluble photosensitizer 5-(4-aminophenyl)-10,15,20-tris- (4-sulphonatophenyl) porphyrin trisodium (see Figure 1). The presence of negatively charged groups on this porphyrin renders it highly water soluble and amenable to its incorporation into hydrophilic scaffold, such as SF.[23–25] The objective of the present work is to demonstrate the ability of hybrid porphyrin-fibroin hydrogels to generate singlet oxygen after gelation.

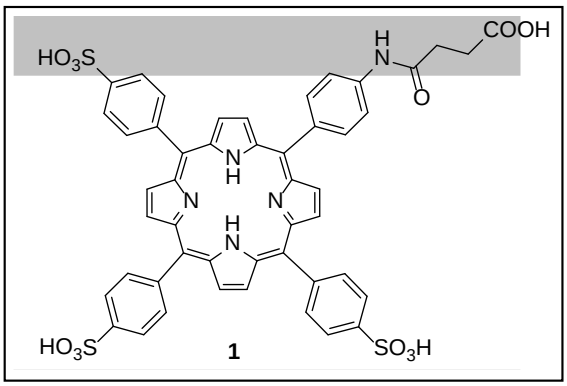

Figure 1. Structure of the photosensitizer 5-(4-aminophenyl)-10,15,20-tris-(4-sulphonatophenyl) porphyrin trisodium used in this study.

Materials and Methods

Materials

All reagents used in this work were of analytical grade. Silk fibroin was extracted from Frisson extra silk (residues from silk processing) from Bractac (Londrina, Brazil). Lithium bromide was purchased from Sigma-Aldrich, and all of the other reagents were obtained from Synth (Brazil). Ultrapure Milli Q water was used in the study. Dialysis membranes with a molecular weight cut-off of 14 kDa were purchased from Sigma-Aldrich.

Preparation of silk fibroin solutions (SFS) and fibroin hydrogels

Fibroin from *Bombyx mori* was isolated from 10 g of raw silk and was degummed by soaking in aqueous 20 mM (1 L) Na_2CO_3 at 85 °C for 30 min to remove the sericin from the fibers, [26,27] followed by rinsing in deionized water 3 times for 20 min after each wash with the salt solution. The fibers were then dried for 24 h at 72 °C. The degummed fibers were dissolved in 9.3 M aqueous LiBr solution by heating at 80 to 100 °C on a hot plate with constant stirring to aid in the dispersion of the fibroin. The solutions obtained were purified by dialysis against water for 48 h to eliminate the salts contained in the solutions and then were centrifuged to eliminate solid residues. The fibroin concentration (61 mg mL^{-1} corresponding to 6.1% w/v) was determined by measuring the residual mass after drying at 37 °C using the Eq. (1),

(Eq. 1)

$$\text{SFS concentration (\%)} = (W_2\text{-}W / W_1\text{-}W) \times 100$$

where W and W_1 represent the plate mass before and after adding 1 mL of silk fibroin solution; W_2 indicates the plate weight after the solution was dried at 60 °C for 4 h. The purified silk solution was stored at 4 °C before use, and in this condition, the solutions were stable for up to one month.

For the formation of silk fibroin hydrogels, we chose fibroin that was extracted from Frisson extra raw fibers. An aqueous ethanol solution (50%, v/v) was added to the SF solution to produce the following volume ratios (μL):1000:0 (SFS1000), 750:250 (SFS750), 500:500 (SFS500) and 250:750 (SFS250); the volumes of SF solution and 50% aqueous ethanol are indicated in μL. After thorough mixing, the solutions were placed in a water bath at 37 °C until gelation occurred. To obtain additional translucid materials, we prepared hydrogels with different SF concentrations by diluting the initial 6.1% w/v SF solution while maintaining the optimal SFS/ethanol proportions as in sample SFS250,

which yield fibroin hydrogels with fibroin concentrations of 15.2, 15.0, 12.5, 10.0, 7.5, 6.2, 5.0 and 2.5 mg mL^{-1}.

Synthesis of 5-(4-aminophenyl)-10,15,20-tris-(4-sulphonatophenyl) porphyrin trisodium.

A solution of 5-(4-aminophenyl)-10,15,20-*tris*-(4-sulphonatophenyl) porphyrin trisodium (600 mg, 0.64 mmol) in DMSO (10 mL) was treated with succinic anhydride (40 mg, 6.40 mmol) and the resulting solution was stirred at room temperature for 20 hours. Ethyl acetate (50 mL) was added to the reaction mixture and the solid was collected by centrifugation. The desired porphyrin was crystallized from methanol/diethyl ether (572 mg, 86% yield).

^{1}H-NMR (d_6-DMSO): 10.46 (s, 1H, COO*H*), 8.87 (bs, 8H, β-pyrrol *H*s), 8.19 and 8.07 (2 bs, 16H, aromatic H), -2.38 (s, 2H, pyrrol N*H*); ^{13}C-NMR (d_6-DMSO): 174.4, 171.1, 148.3, 141.7, 139.8, 136.1, 135.1, 134.2, 124.7, 120.7, 120.1, 120.0, 117.8, 32.0, 29.7; ESI-MS (-ve): m/z 968.36 $[M-H]^-$ (exp: 968.26), 483.69 $[(M-2H)/2]^{2-}$ (exp: 483.56).

Fibroin/porphyrin hydrogel preparation

To obtain hydrogel samples with a final SF concentration of 7.5 mg mL^{-1}, 123 µL of the 6.1% SF solution were diluted with distilled water to obtain a volume of 250 µL. To these solutions various volumes of a 5 mg mL^{-1} (0.005 M) stock solution of porphyrin in 50% v/v aqueous ethanol were added to obtain final porphyrin concentrations of 1, 0.5, 0.25, 0.1, 0.05 and 0.025 mg mL^{-1}. Ethanol was added to the mixture to a final sample volume of 1 mL, which produced a series of 6 samples with a constant SF concentration (7.5 mg mL^{-1}), constant ratio of SF solution and 50% ethanol (SF250) and varying porphyrin concentrations (1.0, 0.5, 0.25, 0.1, 0.05 and 0.025 mg mL^{-1}).

Rheological analysis

Viscoelastic properties of all hydrogels were analyzed using controlled-stress Malvern rheometer (Ki nexus Lab +) equipped with a parallel plate geometry and a sample gap of 0.1 mm at 25 ± 0.1 °C. All measurements were performed in triplicate. Oscillatory analyses were conducted at a constant frequency of 1 Hz and a stress sweep from 0.1 to 10 Pa to determine the viscoelastic region of the sample. A constant shear stress of 1 Pa was later selected to perform the frequency sweep from 0.1 to 20 Hz, which was within the previously determined linear viscoelastic region for all samples, and

the storage (G') and loss (G") moduli were recorded. Continuous testing to analyze the thixotropic properties of the materials was performed using a controlled shear rate procedure in the range from 0.1 to 100 s^{-1} and back, each stage lasting 2 minutes. For the determination of the gel strength (*S*) and viscoelastic exponent (*n*), also called the relaxation exponent, the power law model was used Eq. (2). The variation of the storage modulus (G') at low frequencies in a log-log plot of G" versus frequency follows the power law equation as it is presented in Eq. (2):

(Eq. 2)

$$G' = S \cdot \omega^{n}$$

where G' is the storage modulus, S is the hydrogel strength, ω is the frequency and *n* is the viscoelastic exponent. The *n* and S values allowed the quantitative estimation of the strength of hydrogel structures that can be related to the crosslinking density within the polymer network.

Secondary structure analysis

Absorbance spectra of porphyrin solutions and fibroin/porphyrin hydrogels were recorded using a Varian Carry 50 Bio UV/Vis spectrophotometer. The absorbance was measured over a range of 200–1000 nm for all samples. The freshly prepared hydrogels were analyzed using a sandwich cell with a 0.1 mm optic path for the more concentrated samples. At least three measurements were performed for each sample for consistency.

Fluorescence spectra of porphyrin solutions and fibroin/porphyrin hydrogels were obtained using a Varian Cary Eclipse Fluorescence Spectrophotometer using an excitation wavelength of 400 nm and a spectral window of 450 to 790 nm. A slow scan speed was used with excitation and emission slits set to yield a 5-nm resolution for the porphyrin-fibroin hydrogels.

Circular dichroism (CD) spectra were recorded using a 0.1 mm path length (Hellma Analytics), a quartz sandwich cell, on a Jasco-815 CD spectrophotometer (Jasco Co). All samples were scanned at 25 °C with a 10 s accumulation time at a rate of 200 nm/min under constant N_2 purging. The baseline was corrected using an appropriate buffer solution running under the same conditions (blank) and was subtracted from the experimental spectra.

Scanning electron microscopy (SEM)

Image acquisition was performed using an FEI Inspect F50 scanning electron microscope at the LNNano, Brazilian Nanotechnology National Laboratory (CNPEM, Campinas, Brazil). The images were produced using secondary electrons, a 5-kV voltage, a 3-3.5 mm spot size, a 10-12 mm working distance and gold coating. For metallization, 60 seconds of deposition and 40 mA currents were used. The images were analyzed using the ImageJ program to measure fiber diameters.

Small-angle X-ray scattering (SAXS)

SAXS data were collected using the SAXS 1 beamline at the LNLS, Brazilian Synchrotron Light Laboratory (CNPEM, Campinas, Brazil). Hydrogel samples were loaded into 1.5 mm quartz capillaries at 25 °C. The X-ray wavelength was 1.54 Å and the detection was performed using a Pilatus 300k detector. The sample-to-detector distance was set at 0.77 m, leading to a range that was experimentally accessible (from 0.11 to 4 nm^{-1}) for the modulus of the transfer moment vector, $q = 4\pi \sin(\theta)/\lambda$ (where θ is half the scattering angle). Four frames of 30 seconds each were recorded and averaged before background subtraction. All data were analyzed using Fit2D software.[28]

Generation of reactive oxygen species (ROS)

Determination of the singlet oxygen generation efficiency by the fibroin/porphyrin hydrogels was performed incorporating the fluorescent probe Singlet Oxygen Sensor Green probe (SOSG, Thermo Fisher Scientific) in the hydrogel matrix. Irradiation was performed with red LED light (660 nm, 8 Wcm^{-2}) for 80 s total. Hydrogels containing 7.5 mg mL^{-1} SF alone were used as a blank to confirm that the singlet oxygen was generated by the porphyrin. After 10s cycle of irradiation, the fluorescence of the sample was measured using a Varian Cary Eclipse Fluorescence Spectrophotometer at an excitation of 400 nm and scanning from 450 to 790 nm.

In vitro porphyrin release and permeability studies

The evaluation of in vitro drug release was performed by incubating the fibroin hydrogel (7.5 mg mL^{-1} SFS) with porphyrin (1 mg mL^{-1}) in 15 mL of a PBS buffer in a beaker, pH 7.4 at 37 °C, to determine the release profile of the porphyrin. An aliquot of 1 mL was removed from the receptor recipient at times: 0.5, 1, 3, 5, 7, 9 and 24 hours, the intensity of the absorption were measured by UV/Vis.

The in vitro permeation of porphyrin was determined using Franz's cell apparatus. We used a synthetic membrane (Strat-M® Membrane for Transdermal Diffusion Testing, 25 mm discs, Merck Millipore), a non-animal-based model for transdermal diffusion testing that is predictive of diffusion in human skin, and the circulating water baths were set to 37 ºC. Compartments were clamped together, ensuring that the shiny side of the membrane was facing the donor compartment. The receptor compartment was filled with PBS buffer. When the receptor solution reached 37 ºC, 1 mL of the sample was added. An aliquot of each sample 500 µL was removed from the receptor compartment at times: 0.5, 1, 2, 3, 4, 5, 6, 7, 8, and 24 hours. The porphyrin in solution was measured as described above.

Results and Discussion

Hydrogel formation

We investigated the formation of fibroin hydrogels by varying the SF/ethanol ratio of the solution and the protein concentration. The gelation time was monitored by visual inspection of the samples and by an inversion test (see SI file, Figure S1). Variation of the ethanol content in the sample affected their gelation time (Table S1): at a higher ethanol content the gelation time was considerably shorter.

The fibroin gelation is a natural process that can be accelerated by factors such as pH, temperature, salt concentration and addition of alcohol, which attenuate hydrophobic interactions amongst protein chains. The addition of ethanol to SF solutions dehydrates the protein molecules, increasing the intra- and intermolecular interactions leading to the formation of silk II structures that stabilize the hydrogel.[29,30] The lower dielectric constant of ethanol (24.3 ε_0 at 20 °C) relative to water (80 ε_0 at 20 °C) causes the ethanol to gradually replace water molecules solvating the hydrophobic groups of fibroin.[31–33] The progressive solvation of fibroin by ethanol destabilizes the interactions between SF chains and promotes their rearrangement from a higher-energy random coil to a more stable lower-energy β-sheet,[34] thus initiating the conformational transition that gives rise to the formation of regenerated *Bombyx mori* silk fibroin hydrogels.[35–37]

Rheological analysis

We performed oscillatory analysis of SF hydrogel containing different ratios of SF-to-ethanol to characterize their elastic response component G' (storage modulus) and their viscous response

component G” (loss modulus). (Figure 2). Storage modulus G’ provides information about the energy stored during the deformation of a material (*i.e.*, the stiffness of the material), while the loss modulus G” measures the energy dissipated during the deformation (*i.e.*, the flow or liquid-like behavior of the material). If G” > G’, the material behaves like a viscous liquid, whereas for G’ > G” the behavior is that of an elastic solid. For all the SF hydrogels analyzed, the values of G’ were higher than those of G”, and we observed that the G’ and G” values increased with increasing content of SF.

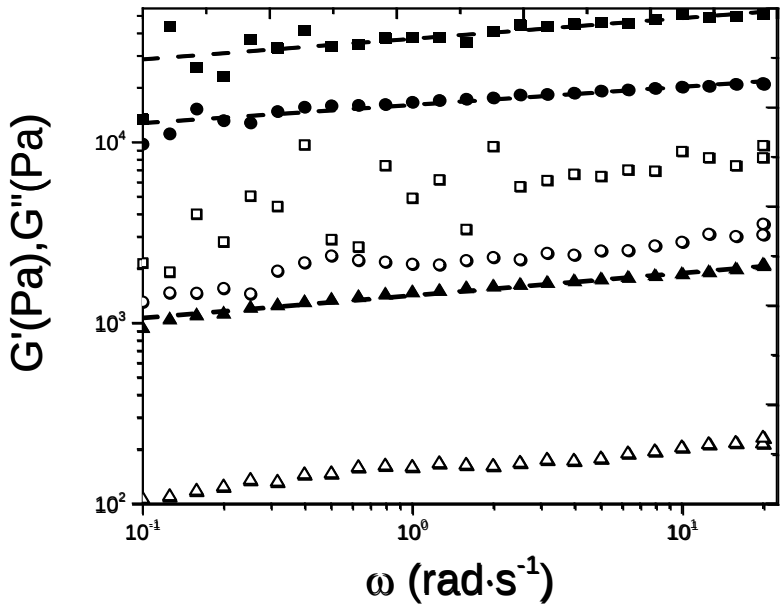

Figure 2. Frequency sweep of the fibroin hydrogels with different porphyrin contents. Closed symbols represent the G’ value and open symbols represent the G” value. SFS750 (circle), SFS500 (square) and SFS250 (diamond). The lines represent the fit of the curve according to the power law model.

We calculated the *n* and S parameters using Equation 1, which yield a quantitative estimation of the strength of the hydrogel structures that can be related to the crosslinking density within the polymer network. With increasing concentrations of SF in the hydrogels we observed increasing values for G’ and S and low *n* exponent values (see Table 1), indicating a higher crosslinking density which results in stronger gel structures. Based on these results, we chose to work with hydrogels with the composition SFS250 (*i.e.*, containing 250 μL of SF solution and 750 μL of 50% aqueous ethanol) due to their shorter gelation time and more favorable rheological properties, and optical properties as transparency (see SI files, Tables S1-S3 and Figure S1).

Table 1. Coefficient of determination for the storage modulus (G’), gel strength (*S*) and viscoelastic exponent (*n*) of the hydrogels obtained.

Hydrogels	**G' (10^3Pa)**	**S (10^3Pa)**	***n***
SFS750	4.10 ± 5.60	4.10 ± 5.60	0.075 ± 0.006

SFS500	1.70± 1.00	1.70 ± 1.00	0.072 ± 0.002
SFS250	1.430 ± 0.02	1.440 ± 0.02	0.118 ± 0.006

The same analysis was performed for the hydrogels containing different concentrations of SF but constant ratios of SF solution and 50% ethanol (SFS250) (Figure S2).

Hydrogels containing higher concentrations of SF exhibited a higher G' value, indicating a stronger and more stabilized hydrogel, and a higher S value, which suggests a higher amount of interchain crosslink (Table 2). Taken together, these results suggest that an increase in SF concentration increases the elastic character of the hydrogel. The hydrogels produced a response that was almost independent of the frequency because this parameter was not dependent on the storage modulus. It is important to note that not all of the hydrogels fit the power-law model: this is because the power-law model is better suited to explain the behavior of pseudo plastic materials,[38] whereas SF hydrogels behave more as a viscoelastic liquid at lower protein concentrations, therefore other models would describe more adequately their rheological behavior.

Table 2. Storage modulus (G'), gel strength (*S*) and viscoelastic exponent (*n*) of the hydrogels. The volume ratio of the SF solution and 50% aqueous ethanol is constant (SFS250)*.

Hydrogel (mg mL^{-1})*	**G'(10^3Pa)**	***S* (10^3Pa)**	***n***
15.2	3.000 ± 1.400	2.1700 ± 0.0600	0.143 ± 0.007
15.0	1.500± 9.600	1.04500 ± 0.0220	0.211 ± 0.005
12.3	0.780 ± 0.070	0.56600± 0.0150	0.178 ± 0.007
10.0	0.330 ± 0.030	0.26100± 0.0060	0.112 ± 0.007
7.5	0.100± 0.010	0.08900± 0.00100	0.098 ± 0.004
5.0	0.030 ± 0.030	0.00500 ± 0.00100	0.730 ± 0.040
2.50	0.002 ± 0.001	0.00016 ± 0.00001	2.080 ± 0.030

Oscillatory analyses were conducted on hybrid fibroin/porphyrin hydrogels (Figure S3): the measurements were performed on a series of samples in which both the concentration of SF (7.5 mg mL^{-1}) and the SF solution/ ethanol volumetric ratio (SFS250) were kept constant, while the concentration of porphyrin varied (namely: 1.0, 0.5, 0.25, 0.1, 0.05 and 0.025 mg mL^{-1}). Hydrogels containing low concentration of porphyrin produced values of G' and G" similar to those of pure fibroin hydrogels. In all cases, the storage modulus G' was higher than the loss modulus G", indicating that the fibroin/porphyrin hydrogels behave like an elastic solid. Visual inspection of the

samples (inversion test) indicated that the presence of the porphyrin did not interfere with the formation of gel nor with the gelation time. Addition of the porphyrin to the hydrogel matrix nevertheless affected the values of G', *S* and *n*, indicating that the rheological properties of the material were slightly modified. At higher concentrations of porphyrin, the G' values of the samples increased with a trend that suggests concentration dependence between the porphyrin content and the storage modulus (Table 3). The values of *S* of the hydrogel also increased, suggesting an enhanced elastic character of the matrix.

Table 3. G' value, gel strength (*S*), viscoelastic exponent (*n*) of fibroin hydrogels (7.5 mg mL^{-1}) and Porod volume with various concentrations of porphyrin (1.0, 0.5, 0.1, 0.05 and 0 mg mL^{-1}).

Porphyrin concentration (mg mL^{-1})	**G'(10^2Pa)**	***S*** **(10^2Pa)**	***n***	**V_{po}**
1.00	5.10 ± 0.60	4.40 ± 0.05	0.095 ± 0.005	154.6
0.50	2.80 ± 0.40	2.40 ± 0.02	0.103 ± 0.004	100.6
0.25	1.80 ± 0.20	1.55 ± 0.01	0.091 ± 0.003	96.8
0.10	1.38 ± 0.14	1.21 ± 0.01	0.082 ± 0.003	90.5
0.05	1.18 ± 0.12	1.04 ± 0.01	0.084 ± 0.003	84.9

The thixotropy behavior of the hydrogels was subsequently investigated. Thixotropic behavior is a desirable feature for materials employed in pharmaceutical and cosmetic preparations, paints and a variety of other applications.[39] Thixotropic materials can be manufactured into an easy-to-handle thick product which becomes a thinner and spreadable material upon application of shear stress.[40] After withdrawal of the stress, the viscosity of the formulation increases preventing its outflow.[41] Agar gels, gelatin gels, iron oxide gels, and certain clays, such as kaolin and bentonite, exhibit thixotropic properties.[42] As shown in Figure 3, all hydrogels (both SF alone and fibroin/porphyrin) behaved as thixotropic materials, as the descending curve does not overlap with the ascending curve, and they exhibited a strong ability to recover their structure once the shear stress was removed. All of the fibroin hydrogels exhibited shear thinning behavior (n<1), as calculated from Equation 2.[43] This behavior indicates that the viscosity of the hydrogel decreases after applying a shear stress to the sample (structure breakdown) and increases again after the stress is removed (structure recovery). The bonds between the molecular structures in these gels are very weak and can be broken by mechanical stress to produce a liquid-like material,[44] which can revert to the gel state by a subsequent rest phase due to the clustering of the particles or by physical cross-linking.

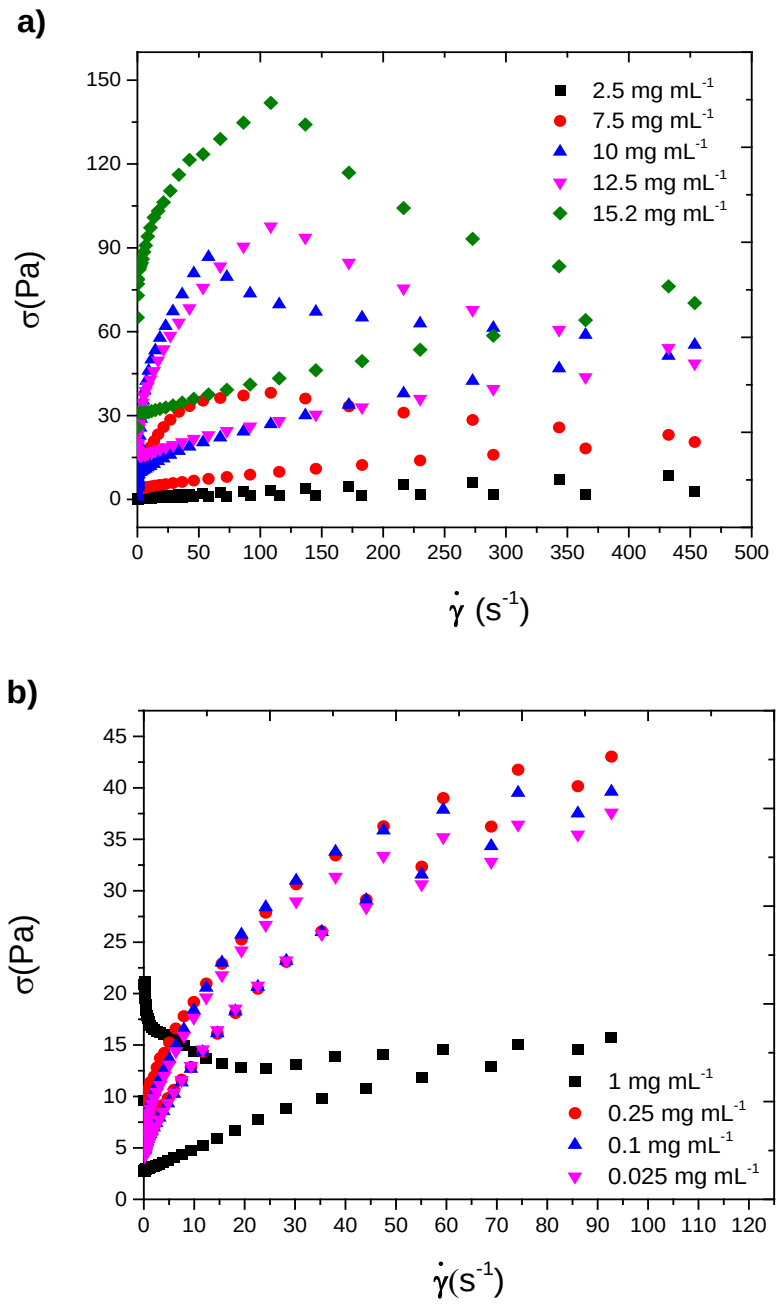

Figure 3. Flow rheograms of hydrogels composed of (a) fibroin and (b) fibroin/porphyrin hydrogels. The flow rheograms shows the thixotropic behavior of the prepared hydrogels; (a) 15.2 mg mL^{-1} (diamond), 12.5 mg mL^{-1} (downside triangle), 10 mg mL^{-1} (triangle), 7.5 mg mL^{-1} (circle) and 2.5 mg mL^{-1} (square); b) 1 mg mL^{-1} (square), 0.25 mg mL^{-1} (circle), 0.1 mg mL^{-1} (triangle) and 0.025 mg mL^{-1} (downside triangle).

SAXS experiments were performed to further characterize structural variations of fibroin/porphyrin (Figure 4). Figure 4a (open symbols) shows the scattering curves of intensity (cm^{-1}) versus the scattering vector q (nm^{-1}) obtained in the absence and in the presence of 1.0 mg mL^{-1} of the porphyrin. All of the experimental results that originated Figure 4a data are available in the supporting information (Figure S4). As observed, the curves are somewhat similar, but the presence of porphyrin promotes an increasing in the slope of the curve at the low angle regions. Indeed, the

intensity decay changes from a ~$q^{-1.6}$ to a ~$q^{-2.1}$ power law (insert Figure 4a), which may be associated with the fractal dimension parameter (D). It is known that D values between 1 and 2 correspond to one-dimensional structures, such as fibers, and two-dimensional structures, such as nanotypes, consistent with a mesh of interwoven fibers, as confirmed by scanning electron microscopy images.[45] To examine this information, Indirect Fourier Transform (IFT) was used to analyze the data. IFT provides information on the studied system in real space through the so-called pair distance distribution function, p(r), and also has the main advantage of being free-modeling (i.e., it does not require any previous information to run). In principle, p(r) could indicate the maximum size of the particle in the system. However, since they are very large (and consequently out of the length scale investigated by SAXS technique), IFT analysis can only provide a qualitative impression regarding the shape of the particles. In this case, from the fitting of the experimental data using IFT (Figure 4b, solid lines), it is possible to conclude that the particles are elongated, and this is compatible with the structures observed by microscopy imaging (Figure S5).

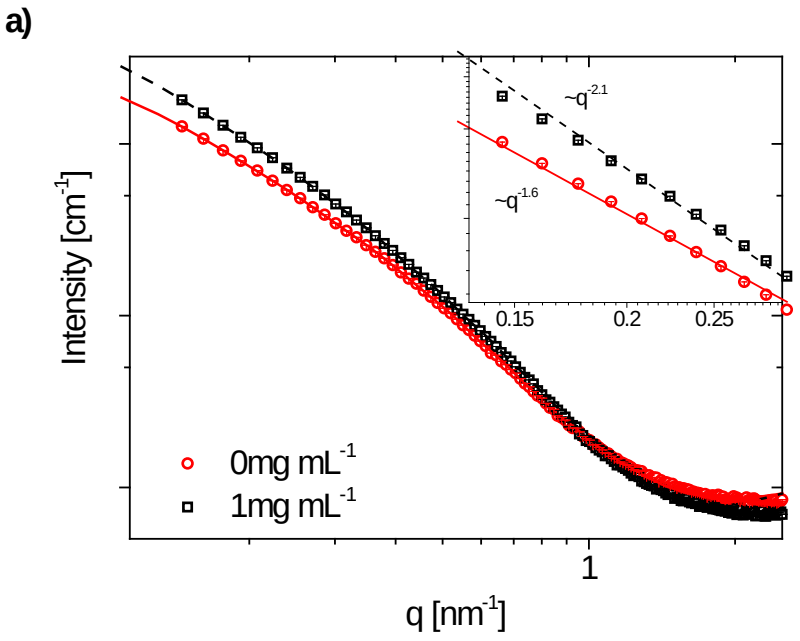

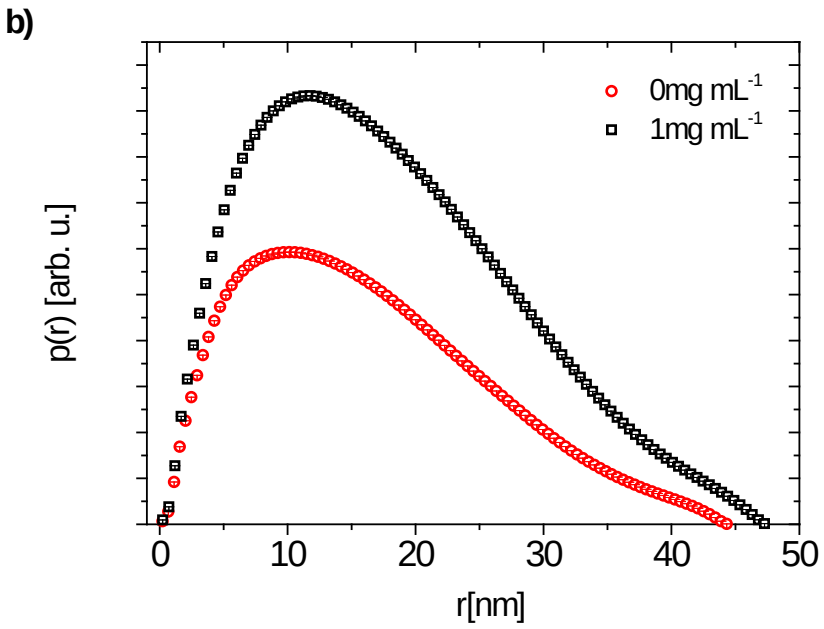

Figure 4. (a) SAXS profiles of fibroin hydrogel with (black open symbols) and without (red circle symbols) porphyrin. Solid lines correspond to fitting using Indirect Fourier Transform (IFT). The inset shows the intensity decay changes at low angle regions; (b) Pair distance distribution function (p(r)) obtained from the IFT fittings.

The Primus program (ATSAS package),[46, 47] was used to calculate the Porod Volume (V_P) for all porphyrin concentrations that were studied (Table 3). This parameter, which is defined as $V_p = \frac{2\pi^2}{Q}$ (where Q is the Porod invariant, for more details see the supporting information),[48] provides insight on the specific volumes of molecules.[49] Increasing the concentration of porphyrin in the hydrogel causes an increase in the V_{po}. The volume of the elongated particles can be altered by increasing their radius or length, as shown in Figure 5. By observing the behavior of the fractal dimension parameter that is obtained in a region of low angle, we can conjecture that the radius of the particle that previously had a linear character subsequently has a more planar behavior with an increase in the amount of porphyrin. At higher V_{po} values, the G' values of is increased, indicating that changes in the concentration of the porphyrin increase the radius of the fibers in the hydrogel and result in a change in the viscosity of the material.

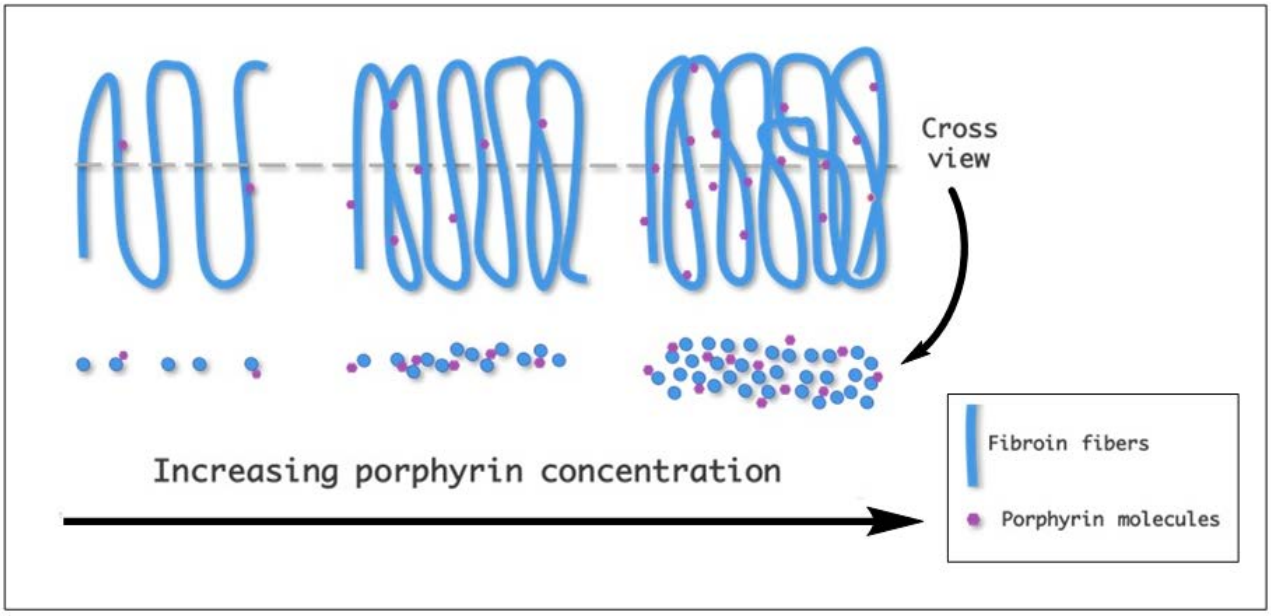

Figure 5. Schematic images (2D and 3D view) illustrating that increasing concentrations of porphyrin causes an increase of the radius of the fibroin fibers in the hydrogel. Cross view: The blue circles represent the fibroin fibers and purple circles porphyrin molecules.

We used the *n* (viscoelastic exponent) and *S* (gel strength) values to provide a better quantitative evaluation of the strength of hydrogels structures that can be related to the crosslinking density within the polymer network. Higher *S* and G' values indicate an increase in the crosslinking density, which is related to stronger gel structures and can be observed in the frequency sweep curve. With an increase in the porphyrin concentration, the storage modulus also increased, resulting in a higher value of *S* (Table 3). Low values of *n* indicate a purely elastic gel behavior.[50]

Increasing the cross-links between the protein chains and/or the fibers affects the physical properties of the hydrogel in relation of the presence and absence of crystallinity. It has been reported that when proteins are irradiated with UV or visible light in the presence of a photosensitizer, both the photo oxidation of sensitive amino acid residues (*i.e.*, cysteine, histidine, tyrosine, methionine and tryptophan) and the formation of covalently cross-linked peptide chains can be observed, which result in the formation of molecular aggregates.[51] This cross-linking has been ascribed to the formation of singlet oxygen *via* a type II photodynamic reaction following the interaction of the excited photosensitizer with triplet oxygen ($^3O_2$) that is present in the surrounding environment. SF has a high content of tyrosine residues (~5%), which can form tyrosine-tyrosine cross-links by photochemical/photodynamic crosslinking.[52] Applegate *et al.* demonstrated that it is possible to form transparent, elastic, silk fibroin hydrogels in which excited riboflavin promotes the formation

of radicals on tyrosine residues, resulting in the formation of tyrosine-tyrosine links between SF chains.[53]

Circular dichroism

The far-UV CD spectra of all the hydrogels were recorded for the hydrogels obtained with the increasing SF concentrations (see Figure 6). The spectrum obtained with 2.5 mg mL^{-1} of SF is typical of a protein the predominance of β-sheet structure with minimum at 217 nm and maximum at 195 nm. The increase of SF concentration led to a red shift of the minimum and maximum wavelength values. Therefore, the far-UV CD spectrum obtained with the lower SF concentration is consistent with a high content of β-sheet structure. The CD spectra of the hydrogel with higher SF concentration progressively deviate from those expected for β-sheet. All the far-UV CD spectra obtained for SF hydrogels are consistent with a contribution of β-sheet structure and confirms that the capacity of ethanol solution with an SFS250 ratio to destabilize the hydrophobic inter- and intramolecular interactions, which results in the aggregation of the protein molecules and in the formation of a stable β-sheet phase.[54,55] In the data of the SF hydrogels containing different concentrations of porphyrin to the matrix, discrete changes in the positive and negative CD bands were observed. The porphyrin-induced CD spectral changes were not linear with the porphyrin concentrations (Figure S6). On the other hand, the CD data showed that none of the porphyrin concentrations used promoted significant destabilization of the SF β-sheet content.

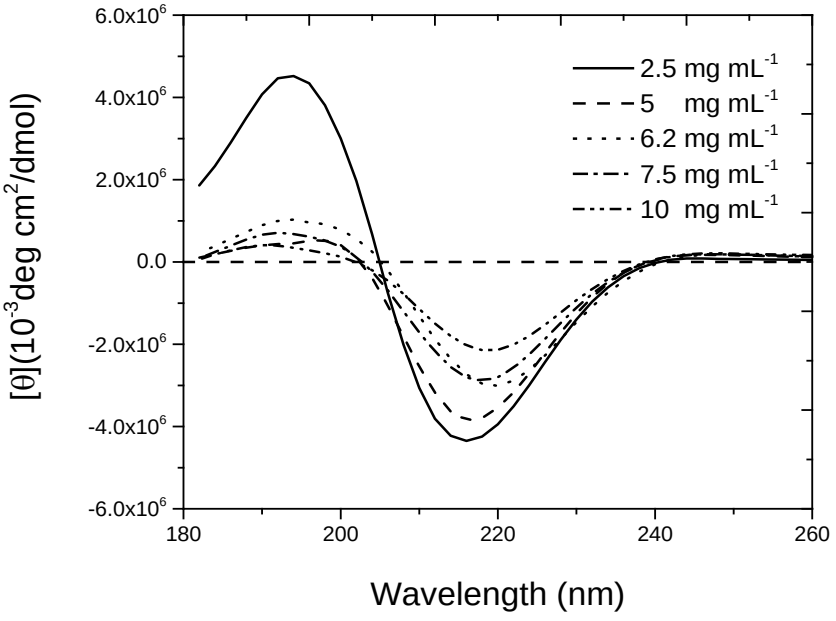

Figure 6. CD spectra of SF hydrogels at different SF concentrations, recorded at 25 °C with a 10 s accumulation time at the rate of 200 nm/min using optical path of 0.012 mm.

Spectroscopic measurements and analysis of the generation of reactive oxygen species

Porphyrins are characterized by a fingerprint UV/Vis spectrum, which consists of a high intensity band peaking at the 400 nm spectral region, the Soret band, and low intensity bands at the 500 nm region, the Q bands. Consistently, the UV/Vis spectrum (Figure S7) of porphyrin solutions displays one band with a high intensity at 416 nm (Soret band) and four other low-intensity signals at 514, 549, 589 and 644 nm (Q bands), which are typical of metal-free porphyrins.[56,57] In the UV/Vis spectrum of SF hydrogels (SFS250, 7.5 mg mL^{-1} SF) with different porphyrin concentrations shows discrete differences in the Q bands, which is consistent with interactions among the porphyrin molecules at higher concentrations. The UV/Vis spectrum of SF hydrogels (SFS250, 7.5 mg mL^{-1} SF) present also a UV band at 274 nm, that was attributed to fibroin absorption (see supporting information). This band is due to absorption by the amino acids contained in the protein, namely tyrosine and tryptophan.[58,59]

The fluorescence spectra of fibroin/porphyrin hydrogels exhibit two bands (Figure S8), one centered at 580 nm and the other one at 640 nm; these signals are characteristic of the porphyrin moiety. The peaks are due to the decay of the porphyrin from an excited electronic state to a ground electronic state (S_1 to S_0 transition).[60] The emission intensity is low at the lower concentrations of porphyrin and no evidence of emission quenching was evident even at the highest concentration of porphyrin. These data do not rule out the existence of a quenching effect of the intensity at concentrations of porphyrin greater than 1 mg $mL^{-1}$of porphyrin.

To evaluate the efficiency of the generation of reactive oxygen species (ROS) by the porphyrin inside the hydrogel matrix, we used the commercially available SOSG as a probe for singlet oxygen. SOSG is a fluorescein-based probe that contains an anthracene moiety. SOSG is highly selective for singlet oxygen and produces no appreciable response to other reactive oxygen species, including the hydroxyl radical ($HO^{\bullet}$), superoxide ($O_2^{\bullet-}$) and nitric oxide (NO). [61] Prior to reaction with singlet oxygen, SOSG exhibits weak blue fluorescence with excitation peaks at 372 and 393 nm and emission peaks at 395 and 416 nm. Following reaction with oxygen, it emits a green fluorescence similar to that of fluorescein (excitation/emission maxima at 504/525 nm).

Upon irradiation of porphyrin-containing SF hydrogels with red light, the fluorescence spectrum of the probe shifted from a weak blue fluorescence to a strong green fluorescence. This behavior

confirmed the generation of singlet oxygen in the material that was generated by the porphyrin *via* a Type II photodynamic process, the Forster energy transfer from the triplet excited porphyrin to the ground state molecular oxygen that is excited to the $^1\Delta$ singlet state.

When comparing the generation of $^1O_2$ in SF hydrogels and in aqueous solutions, we observed that the SOSG fluorescence intensity of the hydrogel containing 0.1 mg $mL^{-1}$of porphyrin is greater than that of an aqueous solution with the same porphyrin concentration, as shown in Figure 7. This higher efficiency of singlet oxygen generation could be due to the reduced aggregation of porphyrin in the hydrogel matrix compared to that in water. Porphyrins often undergo aggregation in water, which results in the formation of π-π stacked aggregates through driving forces such as hydrophobic effects as well as by hydrogen bonding, van der Waals interactions and electrostatic interactions.[62,63] The formation of aggregates results in the quenching of emission, which in some cases limits the applicability of porphyrins as imaging agents. One approach that is used to avoid this quenching is to fix the porphyrin molecule in a 3D network, such as silica or metal organic frameworks, as we demonstrated in this work in the hydrogel matrix.[64]

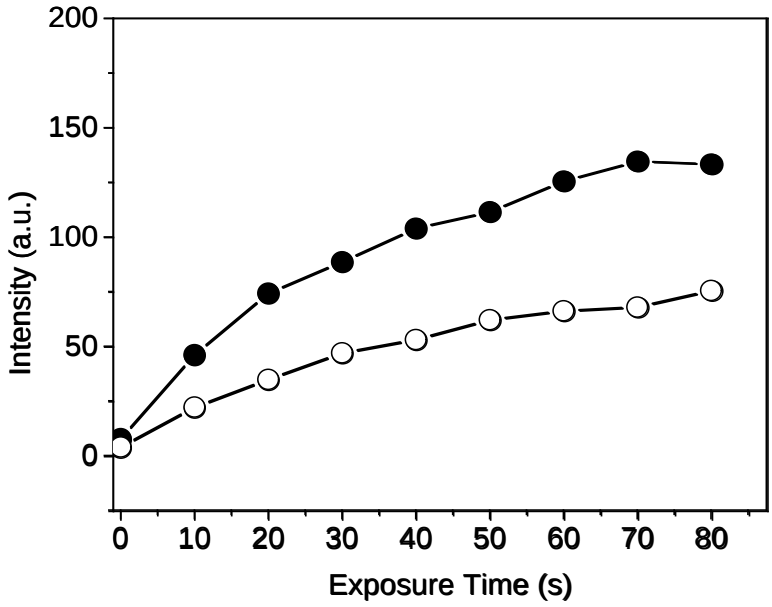

Figure 7. Kinetic curve of the increasing of SOSG fluorescence intensity during the exposure of fibroin/porphyrin hydrogel (close symbol) and porphyrin solution (open symbol) to red light from 0 to 80 s.

This behavior can be ascribed to intermolecular interactions between porphyrin and fibroin. Self-aggregation of porphyrins and other fluorescent molecules is driven by π-π stacking interactions and intermolecular hydrogen bonding.[65] These interactions may be responsible for promoting the association of porphyrins with the fibroin fibers, as it is known that fibroin can form π-π stacking

interactions with aromatic rings by means of tyrosine residues.[66] It has been previously reporter in the literature that curcumin attached to fibroin nanoparticle via π-π stacking and this reduce curcumin release and in our case this mechanism could be possible being the responsible for the silk fibers / porphyrin interactions.[67]

We also investigated the release and permeation of porphyrin from SF hydrogels *in vitro* (Figure 8). For these experiments, we used SFS250 hydrogels containing different concentrations of SF and constant concentration of porphyrin (0.1 mg mL^{-1}). The tests were performed at a constant temperature of 37 °C using a synthetic Strat-M® membrane. This membrane is a non-animal-based model for transdermal diffusion testing that is predictive of diffusion in human skin while limiting lot-to-lot variability. We observed that the porphyrin migrated from the hydrogel through the membrane to the aqueous compartment, where its concentration varied from 0.02 mM to 35 mM. The porphyrin was released slowly from the SF hydrogels due to its high protein concentration: this can be ascribed to the higher viscosity and to the stronger inter- and intramolecular interactions of the more concentrated gel which can limit the diffusion of the porphyrin in the hydrogel.

Our findings indicate that porphyrin is able to diffuse out of the hydrogel and permeate the outer skin layers. The release of porphyrin depends not only on the fibroin concentration but also on the changes in the hydrogel that modify the crosslinking of the matrix, resulting in irregular release profiles. This evidence suggests that SF hydrogels could be used as vehicles for the sustained release of photosensitizers for photodynamic therapy applications. Previous studies have shown that the concentrations of 2 µM and 5 µM of 5,10,15,20-*tetrakis*-(*N*-methyl-pyridinium-4-yl)porphyrin chloride and 5,10,15,20-*tetrakis*-(4-sulfonatophenyl) porphyrin sodium respectively salt inhibit biological processes in tumorigenic cell lines.[68] Concentrations as low as 0.0001 and 2.29 mM of 5,10,15,20-*tetrakis*-phenyl porphyrin induce photokilling of human radial growth phase (RGP) melanoma cells (WM35).[69,70] Additionally, Jing-Jing *et al.*[71] found that concentrations of approximately 6.25 µM of a synthetic porphyrin demonstrated marked phototoxicity towards HGC27 and SNU-1 cells (human gastric cancer cell lines) and the rate of cell death increased significantly in a DTP concentration-dependent and light dose-dependent manner, with maximum mortality rates of 74.14 and 67.76%, respectively.

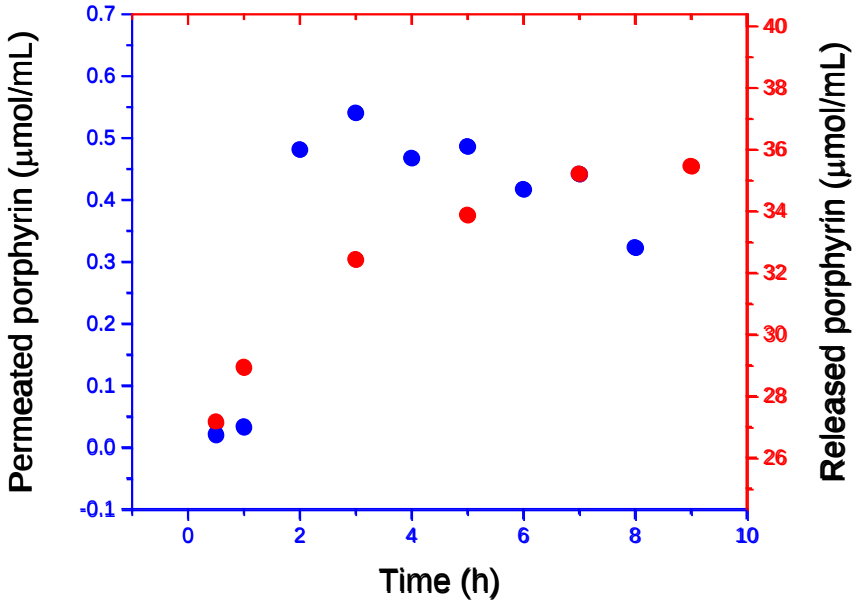

Figure 8. Porphyrin release and permeation profiles. The permeation was performed across a skin-like membrane in a Franz's cell apparatus for 24 h, with a concentration of fibroin of 7.5 mg mL^{-1}. All hydrogels contained 1 mg mL^{-1} of porphyrin. The evaluation of in vitro drug release was performed by incubating the fibroin hydrogel (7.5 mg mL^{-1} SFS) with porphyrin (1 mg mL^{-1}) with 15 mL of a PBS buffer, pH 7.4 at 37 °C.

The concentrations of porphyrin released by the system are comparable to those reported in other studies for example it has been observed that PVA hydrogels are able to release between 0.2 to 0.6 porphyrin (TPPS4) contained in the system. [72] Gonzalez *et al.* also report the release of 5,10,15,20-tetrakis(1-methylpyridinium-4-yl)-porphyrin tetra-iodide (TMPyP) from poly(lactic-co-glycolic acid) (PLGA) nanoparticles, unlike our system these porphyrin particules weren't capable to permeate through the skin model the used in our study [73].

Conclusions

We produced transparent hydrogels containing a range of SF and porphyrin concentrations. Rheological analysis demonstrated that the hydrogels behaved as elastic solids and displayed a shear thinning behavior, which rendered them suitable for biomedical application (e.g., injectable materials). Incorporation of a negatively charged porphyrin in the hydrogels did not interfere with the gelation process, nor did it affect the structure of the gel, as confirmed by rheological analysis and by circular dichroism studies. The hybrid porphyrin/fibroin hydrogels generated singlet oxygen upon irradiation with red light more efficiently than aqueous solutions of porphyrin at equal concentrations. The hydrogel seemingly reduced the aggregation of the porphyrin, enhancing its ability to generate

ROS. We verified that the release of porphyrin from the hydrogel occurred and that its rate could be controlled by altering the concentration of SF in the hydrogel. Our studies led to the conclusion that silk fibroin hydrogels can be used as vehicles for the formulation and release of therapeutic agents for photodynamic therapy. Silk fibroin hydrogels have demonstrated a distinct efficacy as matrices for the incorporation of new functional molecules for biomedical application.

Conflicts of interest

The authors declare no conflicts of interest.

Supporting Information

Rheological parameters, SAXS modelling, fitting parameters, scattering curves, SEM images, CD and UV/Vis data.

Author information

*Corresponding Author E-mail: wendel.alves@ufabc.edu.br. Tel.: +55 11 4996 0193. Fax: +55 11 4996 3166.

Acknowledgments

This work was supported by FAPESP (grant nos. 2015/24018-1, 2014/18527-8 and 2017/02317-2) and CNPq (grant no. 302923/2015-2). INCT in Bioanalytics (FAPESP grant no. 2014/50867-3 and CNPq grant no. 465389/2014-7) are gratefully acknowledged for their grants. J.E.U.R. is grateful to CAPES for a doctoral fellowship. B.B.G. acknowledges FAPESP (project number 2018/05888-3) for a postdoctoral fellowship. FG acknowledges the FAPESP (project number 2014/50972-1) for a Newton Mobility grant. The staff at LNNano and LNLS are gratefully recognized for invaluable help and access to the SEM and SAXS facilities, respectively. Dr. Emerson Rodrigo da Silva (Biophysics Dept, UNIFESP) is kindly acknowledged for providing access and assistance during the circular dichroism experiments. The authors are grateful to the Multiuser Central Facilities at UFABC.

References

[1] F. Galeotti, A. Andicsova, S. Yunus, C. Botta, *Soft Matter* **2012**, *8*, 4815.

[2] C. Vepari, D. L. Kaplan, *Prog. Polym. Sci.* **2007**, *32*, 991.

[3] B. Kundu, R. Rajkhowa, S. C. Kundu, X. Wang, *Adv. Drug Deliv. Rev.* **2013**, *65*, 457.

[4] A. Motta, C. Migliaresi, F. Faccioni, P. Torricelli, M. Fini, R. Giardino, *J. Biomater. Sci. Polym. Ed.* **2004**, *15*, 851.

[5] M. Ciocci, I. Cacciotti, D. Seliktar, S. Melino, *Int. J. Biol. Macromol.* **2018**, *108*, 960.

[6] S. Yan, Q. Wang, Z. Tariq, R. You, X. Li, M. Li, Q. Zhang, Q. Wang, Z. Tariq, R. You, X. Li, M. Li, Q. Zhang, *Int. J. Biol. Macromol.* **2018**,*118*, 775.

[7] F. Ullah, M. B. H. Othman, F. Javed, Z. Ahmad, H. M. Akil, *Mater. Sci. Eng. C* **2015**, *57*, 414.

[8] S. F. Souza, S. Kogikoski Jr., E. R. Silva. W. A. Alves, *J. Braz. Chem. Soc.*. **2017**, *28*, 1619.

[9] J. Jin, V. Reese, R. Coler, D. Carter, M. Rolandi, *Adv. Healthc. Mater.* **2014**, *3*, 349.

[10] A. Kawczyk-Krupka, A. M. Bugaj, W. Latos, K. Zaremba, K. Wawrzyniec, A. Sieroń, *Photodiagnosis Photodyn. Ther.* **2015**, *12*, 545.

[11] Y. Wang, B. Han, R. Shi, L. Pan, H. Zhang, Y. Shen, C. Li, F. Huang, A. Xie, *J. Mater. Chem. B* **2013**, *1*, 6411.

[12] Y. Chang, X. Li, L. Zhang, L. Xia, X. Liu, C. Li, Y. Zhang, *Sci. Rep.* **2017**,*7*, 45633.

[13] K. Marta, K. Patrycja, J. Kimball, M. Rojkiewicz, P. Kus´, Z. Gryczynski, A. Ratuszna, *Spectrochim. Acta Part A Mol. Biomol. Spectrosc.* **2015**, *146*, 249.

[14] S. Clement, W. Deng, E. Camilleri, B. C. Wilson, E. M. Goldys, *Sci. Rep.* **2016**, *6*, 19954.

[15] P. Kumari, R. Gautam, A. Milhotra, *Chem. Biol. Lett.* **2016**, *3*, 32.

[16] Y. I. Svenskaya; A. M. Pavlov; D. A. Gorin; D. J. Gould; B. V. Parakhonskiy; G. B. Sukhorukov. Colloids Surfaces B Biointerfaces **2016**, *146*, 171

[17] Q. Zou; M. Abbas; L. Zhao; S. Li; G. Shen; X. Yan. J Am Chem Soc **2017**, *139*, 1921.

[18] K. Liu; R. Xing; Q. Zou; G. Ma; H. Möhwald; X. Yan. Angew Chemie - Int Ed **2016**, *55*, 3036.

[19] S. Li; Q. Zou; Y. Li; C. Yuan; R. Xing; X. Yan. J Am Chem Soc **2018**, *140*, 10794

[20] E. J. Hong, D. G. Choi, M. S. Shim, *APBS*, **2016**, *6*, 297

[21] E. Moser, A. T. Eggebrecht, M. S. Patterson, J. F. Lovell, H. Huang, W. Song, J. Rieffel,

Front. Phys. **2015**, *8*, 155.

[22] A. N. Mitropoulos, B. Marelli, C. E. Ghezzi, M. B. Applegate, B. P. Partlow, D. L. Kaplan, F. G. Omenetto, *ACS Biomater. Sci. Eng.* **2015**, *1*, 964.

[23] K. W. Hipps, U. Mazur, *Langmuir* **2018**, 34,3.

[24] J.-H. Fuhrhop, *Langmuir***, 2014**, *30*, 1.

[25] P. Guo, P. Chen, M. Liu, *Langmuir* **2012**, *28*, 15482.

[26] D. N. Rockwood, R. C. Preda, T. Yücel, X. Wang, M. L. Lovett, D. L. Kaplan, *Nat. Protoc.* **2011**, *6*, 1612.

[27] D. Su, M. Yao, J. Liu, Y. Zhong, X. Chen, Z. Shao,**2017,** *9*, 17489.

[28] A. P. Hammersley, FIT2D, **1997**.

[29] M. Ribeiro, M. A. de Moraes, M. M. Beppu, F. J. Monteiro, M. P. Ferraz, *Biomatter*, **2014**, *4*, e28536.

[30] K. Kaewprasit, T. Kobayashi, S. Damrongsakkul, *Int. J. Biol. Macromol.*,**2018**,*118*, 1726.

[31] V. Calandrini, D. Fioretto, G. Onori, A. Santucci, *Chem. Phys. Lett.* **2000**, *324*, 344.

[32] I. W. Fu, C. B. Markegard, B. K. Chu, H. D. Nguyen, *Langmuir* **2014**, *30*, 7745.

[33] Q. Lu, H. Zhu, C. Zhang, F. Zhang, B. Zhang, D. L. Kaplan, *Biomacromolecules* **2012**, *13*, 826.

[34] Y. Wang, J. Wen, B. Peng, B. Hu, X. Chen, Z. Shao, *Biomacromolecules* **2018**, *19*, 1999.

[35] S. S. Silva, E. G. Popa, M. E. Gomes, M. B. Oliveira, S. Nayak, B. Subia, J. F. Mano, S. C. Kundu, R. L. Reis, *Acta Biomater.* **2013**, *9*, 8972.

[36] X. Hu, D. Kaplan, P. Cebe, *Macromolecules* **2008**, *41*, 3939.

[37] M. C. Bellissent-Funel, A. Hassanali, M. Havenith, R. Henchman, P. Pohl, F. Sterpone, D. Van Der Spoel, Y. Xu, A. E. Garcia, *Chem. Rev.* **2016**, *116*, 7673.

[38] B. P. Partlow; M. Bagheri; J. L. Harden; D. L. Kaplan. Biomacromolecules **2016**, *17*, 3570

[39] G. Calixto, A. C. Yoshii, H. R. Silva, B. S. F. Cury, M Chorilli, *Pharm. Dev. Technol.* **2015**, *20*, 490.

[40] J. Nanda, A. Biswas, A. Banerjee, *Soft Matter* **2013**, *9*, 4198.

[41] Y. Liu, S. Ling, S. Wang, X. Chen, Z. Shao, *Biomater. Sci.* **2014**, *2*, 1338.

[42] Y. Wan, L. Liu, S. Yuan, J. Sun, Z. Li, *Langmuir* **2017**, *33*, 6.

[43] T. D. Hamilton, D. Bucar, J. Baltrusaitis, D. R. Flanagan, *J. Am. Chem. Soc.* **2011**, *133*, 3365.

[44] S. Rammensee, K. D. Hermanson, A. R. Bausch, *Appl. Phys. A* **2006**, *82*, 261.

[45] P. V Konarev; V. V Volkov; A. V Sokolova; M. H. J. Koch; D. I. Svergun, *J Appl Cryst.*, **2003**, *36*, 1277.

[46] A. Rekas; V. Lo; G. E. Gadd; R. Cappai; S. I. Yun. Macro **2009**, *9*, 230.

[47] D. Franke, D. Petoukhov, M.V. Konarev, P.V. Panjkovich, A. Tuukkanen, A. Mertens, H.D.T., Kikhney, A.G., Hajizadeh, N.R., Franklin, J.M., Jeffries, C.M. and Svergun, *J. Appl. Cryst*, **2017**, *50*, 1212.

[48] J. Liu, S. Pancera, V. Boyko, A. Shukla, T. Narayanan, K. Huber, *Langmuir* **2010**, *26*, 17405.

[49] J. L. Whittaker, R. Balu, R. Knott, L. De Campo, J. P. Mata, C. Rehm, A. J. Hill, N. K. Dutta, N. Roy, *Int. J. Biol. Macromol.* **2018**, *114*, 998.

[50] Y. Tao, A. Hasan, G. Deeb, C. Hu, H. Han, *Polymers* **2016**, *8*, 94.

[51] B. P. Partlow, M. B. Applegate, F. G. Omenetto, D. L. Kaplan, *ACS Biomater. Sci. Eng.* **2016**, *2*, 2108.

[52] Y. Ding, Y. Li, M. Qin, Y. Cao, W. Wang, *Langmuir* **2013**, *29*, 13299.

[53] M. B. Applegate, B. P. Partlow, J. Coburn, B. Marelli, C. Pirie, R. Pineda, D. L. Kaplan, F. G. Omenetto, *Adv. Mater.* **2016**, *28*, 2417.

[54] M. A. De Moraes, C. R. A. Mahl, M. F. Silva, M. M. Beppu, *J. Appl. Polym. Sci.* **2015**, *132*, 41802.

[55] S. Y. Cho, Y. S. Yun, S. Lee, D. Jang, K. Park, J. K. Kim, B. H. Kim, K. Kang, D. L. Kaplan, H. Jin, *Nat. Commun.* **2015**, *6*, 7145.

[56] M. Pérez-Morales, G. de Miguel, H. J. Bolink, M. T. Martín-Romero, L. Camacho, *J. Mater. Chem.* **2009**, *19*, 4255.

[57] Y. Wan, Y. Xue, N. Sheng, G. Rui, C. Lv, J. He, B. Gu, Y. Cui, *Opt. Laser Technol.* **2018**, *102*, 47.

[58] C. Hazra, T. Samanta, V. Mahalingam, *J. Mater. Chem. C Mater. Opt. Electron. devices*, **2014**, *2*, 10157–10163.

[59] J. M. Antosiewicz, D. Shugar, *Biophys. Rev.* **2016**,*8*, 163–177.

[60] M. Bala Murali Krishna, N. Venkatramaiah, R. Venkatesan, D. Narayana Rao, *J. Mater. Chem.* **2012**, *22*, 3059.

[61] S. Kim, M. Fujitsuka, T. Majima, *J. Phys. Chem. B* **2013**, *117*, 13985.

[62] B. Guo, X. Cai, S. Xu, S. M. A. Fateminia, J. Liu, J. Liang, G. Feng, W. Wu, B. Liu, *J.*

Mater. Chem. B **2016**, *4*, 4690.

[63] S. M. Andrade, S. M. B. Costa, *Chem. - A Eur. J.* **2006**, *12*, 1046.

[64] C. P. Ponce, H. Y. Araghi, N. K. Joshi, R. P. Steer, M. F. Paige, *Langmuir* **2015**, *31*, 13590.

[65] X. Ma; R. Sun; J. Cheng; J. Liu; F. Gou; H. Xiang; X. Zhou. J Chem Educ **2016**, 93, 345.

[66] B. P. Partlow; M. Bagheri; J. L. Harden; D. L. Kaplan. Biomacromolecules 2016, 17, 3570

[67] O. Gianak; E. Pavlidou; C. Sarafidis; V. Karageorgiou; E. Deliyanni. Separations **2018**, 5, 25

[68] S. P. S. Tita, J. R. Perussi, *Brazilian J. Med. Biol. Res.* **2001**, *34*, 1331.

[69] I. Baldea, D. Elena, P. Bolfa, R. Mariana, N. Decea, M. Cenariu, M. Banciu, A. Viorica, A. Gabriela, *J. Photochem. Photobiol. B Biol.* **2015**, *151*, 142.

[70] I. Baldea, R. Ion, E. D. Olteanu, I. Nenu, *Clujul Med.* **2015**, *88*, 175.

[71] J.J. Chen, L.-J. Gao, T.-J. Liu, *Oncol. Lett.* **2016**, *11*, 775.

[72] B. Peter. CIM Mag **2017**, *12*, 40.

[73] J. A. González-Delgado; P. M. Castro; A. Machado; F. Araújo; F. Rodrigues; B. Korsak; M. Ferreira; J. P. C. Tomé; B. Sarmento. Int J Pharm **2016**, *510*, 221